Mon. Not. R. Astron. Soc. **000**, 000–000 (0000) Printed 9 August 2008 (MN LaTeX style file v2.2)

arXiv:0704.3739v3 [astro-ph] 9 Aug 2008

Luminous Red Galaxy Clustering at $z \simeq 0.7$ - First Results using AAOmega

Nicholas P. Ross[⋆1,2], T. Shanks[1], Russell D. Cannon[3], D.A. Wake[1], R. G. Sharp[3], S. M. Croom[4] and John A. Peacock[5]

[1] *Physics Department, Durham University, South Road, Durham, DH1 3LE, UK*
[2] *Department of Astronomy and Astrophysics, The Pennsylvania State University, 525 Davey Laboratory, University Park, PA 16802, U.S.A.*
[3] *Anglo-Australian Observatory, PO Box 296, Epping, NSW 1710, Australia*
[4] *School of Physics, University of Sydney, Sydney, NSW 2006, Australia*
[5] *SUPA, Institute for Astronomy, University of Edinburgh, Royal Observatory, Blackford Hill, Edinburgh EH9 3HJ*

9 August 2008

ABSTRACT

We report on the AAT-AAOmega LRG Pilot observing run to establish the feasibility of a large spectroscopic survey using the new AAOmega instrument. We have selected Luminous Red Galaxies (LRGs) using single epoch SDSS *riz*-photometry to $i < 20.5$ and $z < 20.2$. We have observed in 3 fields including the COSMOS field and the COMBO-17 S11 field, obtaining a sample of ∼600 redshift $z \gtrsim 0.5$ LRGs. Exposure times varied from 1 - 4 hours to determine the minimum exposure for AAOmega to make an essentially complete LRG redshift survey in average conditions. We show that LRG redshifts to $i < 20.5$ can measured in ≈1.5hr exposures and present comparisons with 2SLAQ and COMBO-17 (photo-)redshifts. Crucially, the *riz* selection coupled with the 3-4× improved AAOmega throughput is shown to extend the LRG mean redshift from z=0.55 for 2SLAQ to $z = 0.681 \pm 0.005$ for *riz*-selected LRGs. This extended range is vital for maximising the S/N for the detection of the baryon acoustic oscillations (BAOs). Furthermore, we show that the amplitude of LRG clustering is $s_0 = 9.9 \pm 0.7 \;\; h^{-1}$ Mpc, as high as that seen in the 2SLAQ LRG Survey. Consistent results for this clustering amplitude are found from the projected and semi-projected correlation functions. This high amplitude is consistent with a long-lived population whose bias evolves as predicted by a simple "high-peaks" model. We conclude that a redshift survey of 360 000 LRGs over 3000 deg^2, with an effective volume some 4× bigger than previously used to detect BAO with LRGs, is possible with AAOmega in 170 nights.

Key words: galaxies - luminous red, surveys: clustering - large-scale structure: evolution - clustering.

1 INTRODUCTION

Large-scale structure (LSS) studies are one road into investigating "Dark Energy" (DE) and its potential evolution (e.g. Blake & Glazebrook 2003; Seo & Eisenstein 2003, 2005, 2007; Angulo et al. 2008). This has been powerfully demonstrated by recent results from the Luminous Red Galaxy (LRG) Sloan Digital Sky Survey (SDSS), (e.g. Eisenstein et al. 2005; Tegmark et al. 2006; Percival et al. 2007a,b) and indeed the 2dFGRS (Cole et al. 2005). Luminous Red Galaxies (LRGs) are predominantly massive early-type galaxies and are intrinsically luminous ($\gtrsim 3L^{*}$) (Eisenstein et al. 2003; Loh & Strauss 2006; Wake et al. 2006). They are strongly biased objects, having values of $b \sim 2$, (Padmanabhan et al. 2007) where b is the linear bias and relates, in the linear regime, the underlying mass density distribution to that of the luminous tracers via $\delta_g = b\,\delta_m$. As such and coupled to their very clean and efficient selection, LRGs are excellent tracers of large-scale structure and can be used as cosmological probes. Eisenstein et al. (2005), Tegmark et al. (2006), Hütsi (2006), Percival et al. (2007a) and Percival et al. (2007b) use positions and spectroscopic redshifts from the SDSS LRG Survey in order to accurately measure the correlation function and the Power Spectrum. Specifically, a detection of the baryon acoustic oscillations (BAOs) in the galaxy distribution is made. BAOs in the

---

[⋆] email: Nicholas.Ross@durham.ac.uk

Field Name	R.A. (J2000)	Dec (J2000)	No. of exposures	Average seeing($''$)					Average airmass				
COSMOS	10h 00m 28.6s	02d 12m 21.0s	0+7+0+6+0	–	2.0	–	3.0	–	–	1.39	–	1.27	–
COMBO-17 S11	11h 42m 58.0s	−01d 42m 50.0s	2+6+4+0+9	2.0	1.8	1.7	–	1.9	1.15	1.19	1.21	–	1.19
2SLAQ d05	13h 21m 36.0s	−00d 12m 35.0s	8+0+0+5+0	1.9	–	–	1.6	–	1.22	–	–	1.19	–

Table 1. The 3 AAOmega LRG Pilot fields. The fourth column gives the number of 1200 second exposures on the 5 consecutive nights of the pilot run, 03 March 2006 through 07 March 2006. Note that the 9 exposures taken in the S11 field on the night of 07 March 2006 targeted objects which had a z-band magnitude selection of $19.5 < z < 20.2$.

galaxy distribution are caused by sound waves propagating through the baryon-photon plasma in the early ($z > 1100$) Universe. At recombination, these sound waves are "frozen" into the distribution of matter at a preferred scale (see e.g. Eisenstein & Hu 1998; Meiksin et al. 1999; Yamamoto et al. 2006; Eisenstein et al. 2007, for further BAO details). With measurements of the BAOs now starting to appear feasible, there is a push to carry out large galaxy surveys at higher redshift, with the primary goal of tracking the evolution of dark energy and the related equation of state parameter, $w_{\rm DE}(z)$, over cosmic time. As such, several new galaxy redshift surveys have been proposed. One possibility is to use the AAOmega spectrograph at the AAT to make a spectroscopic redshift survey of high redshift LRGs based on both SDSS Equatorial imaging, as well as new imaging from the 2.6m VLT Survey Telescope (VST). AAOmega retains the fibre-fed multi-object capability across a wide field-of-view from the old 2dF instrument but the top-end spectrographs have been replaced with a new single bench mounted spectrograph, with a red and a blue arm. Sharp et al. (2006) gives complete instrument details. In this paper we present the results from an AAOmega LRG redshift survey. Although the primary driver for this survey is as a "Pilot" study to investigate the nature of dark energy at high redshift via the BAOs, there are also several other areas of interest. By comparing clustering results at $1 < r < 10$ h^{-1} Mpc scales from low ($z < 0.4$), intermediate ($z = 0.55$), and high ($z \sim 0.7$), redshift LRG studies (Zehavi et al. 2005; Ross et al. 2007, and this study respectively) we can begin to learn about the formation and evolution of the most massive galaxies, and hence, potentially the most massive dark matter haloes, from high redshift.

The layout of the paper is as follows. In Section 2 we describe the selection criteria used to select our high redshift LRGs. In Section 3 we give a brief overview of the instrument set-up used and report on the redshift statistics for our survey, including example spectra. In Section 4 we present our clustering results and in Section 5 we discuss our results in the context of other recent results using a simple Halo Occupation Distribution (HOD) model. We conclude in Section 6. We assume a flat ΛCDM cosmology, with $(\Omega_{\rm m}, \Omega_\Lambda)$=(0.3,0.7) throughout, unless otherwise explicitly stated. We quote distances in terms of h^{-1} Mpc, where h is the dimensionless Hubble constant such that $H_0 = 100h$ km s^{-1} Mpc^{-1}.

2 SDSS LRG SELECTION

At its heart the AAOmega LRG Pilot relies on single-epoch photometric data from the SDSS (York et al. 2000; Gunn et al. 2006) to provide targets for the recently commissioned AAOmega instrument on the 3.9m Anglo-Australian Telescope (AAT).

The target selection was designed to select high-redshift LRGs out to $z \simeq 1$ with a mean redshift of $z \simeq 0.7$. Using the SDSS Data Release 4 (DR4; Adelman-McCarthy et al. 2006), we extracted photometric data for objects classified as galaxies. Three different selections were then applied to the downloaded data, with the selections being designed to recover a target sky density of ~ 90 objects per square degree.

First, we repeat the *gri*-band based selection that was used in the 2SLAQ LRG Survey. We will not repeat the full selection criteria here (the reader is referred to Cannon et al. (2006) for further details) but note that LRGs are selected in the $(g-r)$-$(r-i)$ colour-colour plane with $17.5 < i_{\rm deV} < 19.8$, where $i_{\rm deV}$ is the i-band de Vaucouleurs magnitude.

Now with the aim of measuring significantly higher redshifts than the 2SLAQ LRG Survey ($\bar{z}_{\rm 2SLAQ} = 0.55$), two further selections were carried out, this time in the $(r-i)$-$(i-z)$ colour-colour plane. The first *riz*-selection had objects in the magnitude range $19.8 < i_{\rm deV} < 20.5$, while the second *riz*-selection had objects in the magnitude range $19.5 < z < 20.2$, where z is the SDSS "Model" magnitude (Fukugita et al. 1996; Stoughton et al. 2002). These magnitude ranges were based on experience gained from the 2SLAQ LRG Survey as well as the expected performance of the new AAOmega instrument, such that LRGs with a significantly higher redshift than the previous survey could be selected and observed in a relatively short exposure (~ 1.5 hours). Within these two *riz*-band selections, objects were assigned different observational priorities. The line "$e_{\parallel}$"was defined (continuing on from, but not directly related to $c_{\parallel}$ in Eisenstein et al. (2001) and $d_{\parallel}$ in (Cannon et al. 2006)), as

$$e_{\parallel} = (i-z) + \frac{9}{7}(r-i) \geq 2.0. \tag{1}$$

and is used to define a boundary in the *riz*-plane. (All colours reported here, such as those given in Equation 1, are again based on "Model" magnitudes). A higher priority *riz*-plane cut was imposed with

$$0.5 \leq (r-i) \leq 1.8, \tag{2}$$

$$0.6 \leq (i-z) \leq 1.5, \tag{3}$$

$$e_{\parallel} \geq 2.0. \tag{4}$$

The lower priority cut has

$$0.2 \leq (i - z) \leq 0.6, \qquad (5)$$

$$x \leq (r - i) \leq 1.8, \qquad (6)$$

where x was the smaller of $e_{\|}$ and 1.2 at the given $(i - z)$. These cuts can be seen in Figure 1 where the two priorities are shown by the regions marked A and B. The two evolutionary tracks in Figure 1 the stellar population synthesis code based on Bruzual & Charlot (2003). The solid line being a "single burst" model, where star formation occurs in a single instantaneous burst at high redshift and then has the stellar population evolving passively. The dashed line on the other hand is based on a model with continuous star formation, with the timescale of star formation given as $\tau = 1$ Gyr, where τ is a decay constant in that the star formation rate (SFR) is $\propto \exp^{-t/\tau}$. Both models assume a Salpeter IMF (Salpeter 1955) with solar metallicity and a galaxy formation redshift of $z_{\mathrm{form}} = 10$. The evolutionary tracks start near $(r - i) = (i - z) = 0.4$ for zero redshift, turn upwards near $(r - i) = 1.3$ corresponding to redshift $z = 0.7$ and then turn down again near $(i - z) \sim 1.1$ corresponding to redshift $z = 1.0$. These turning points correspond to the CaII H+K 4000Å break moving into the i- and z-bands respectively. The solid circles show the colour evolution at redshift z =0.0, 0.5, 1.0 and 1.5.

3 AAOMEGA SPECTROSCOPY

3.1 Observational Details

Observations were made on the nights of 03 March 2006 to 07 March 2006 inclusive; the first three nights were Dark nights, the last two were Grey nights. Of these nights, a total of $\simeq 2$ were lost to cloud and seeing was frequently poor on the others (see Table 1). We observed in 3 fields, with a total area of $\simeq 10$ deg^2, including the COSMOS field (Scoville et al. 2007), the COMBO-17 S11 field (Wolf et al. 2003) and a previously observed 2SLAQ Survey field, d05 (Cannon et al. 2006), the coordinates of which are also given in Table 1. For reference, the COSMOS Survey has an area of 2 deg^2, the COMBO-17 S11 field is 0.26 deg^2 in coverage, while the 2SLAQ LRG Survey has an effective area of 135 deg^2 (Sec. 7.2, Cannon et al. 2006).

All data were taken with the same spectrograph set-up. The 5700Å dichroic was used. For the red arm spectrograph the 385R grating was centred at 7625Å; for the blue arm spectrograph the 580V grating was centred at 4800Å. However, no blue arm data was used in our analysis as the S/N was low, as expected for red galaxies.

Data reduction was performed using the 2dF data reduction pipeline software, `2dfdr` (Bailey et al. 2005) and the redshifts were derived using ZCODE developed by Will Sutherland and others for the 2dFGRS Survey (Colless et al. 2001, and references therein). The modifications to ZCODE originally made for the higher redshift $z \sim 0.5$ galaxies in the 2SLAQ LRG Survey were retained. The final catalogue from the AAOmega LRG Pilot contains 1270 unique galaxy spectra with 804 objects having reliable "Qop ≥ 3"[1] redshifts, see Table 2. Of these, 217 objects had M-type stellar spectra leaving 587 high-redshift LRGs. The COSMOS field contributed 156 LRGs out of 321 obtained spectra, the 2SLAQ d05 field 177/345 and the S11 field 254/604. The greater number of spectra obtained in S11 was due to the fact that objects in the field were targeted not only with the $19.8 < i < 20.5$ selection but also with the $19.5 < z < 20.2$ z-band selection.

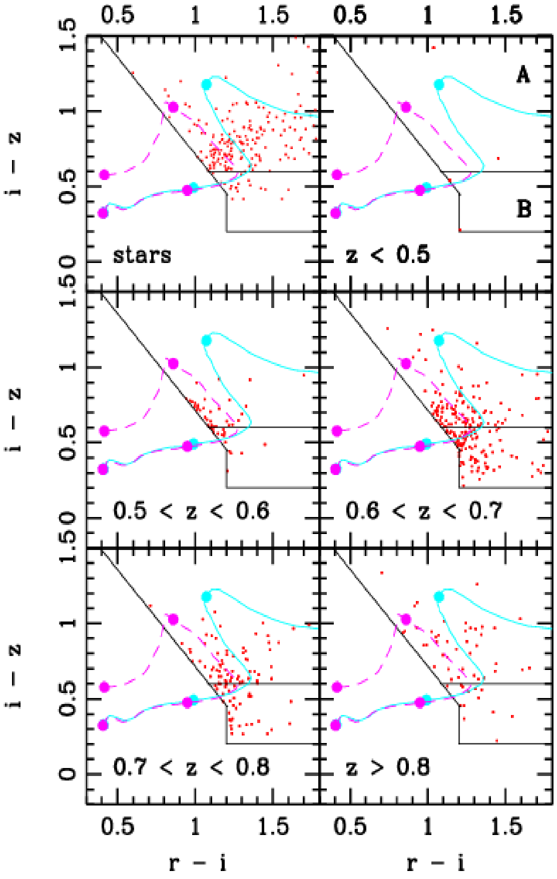

Figure 1. The selection of $z \sim 0.7$ LRGs using the SDSS riz-bands. The (red) dots are objects with confirmed spectroscopic redshifts for both the $19.8 < i_{\mathrm{deV}} < 20.5$ and $19.5 < z < 20.2$ magnitude selections. The tracks are Bruzual & Charlot models, details given in the text with the solid (cyan) line being a "single burst" model and the dashed (magenta) line having being a τ=1 Gyr model. The diagonal lines are $e_{\|} = 2.0$. The area labelled "A" in the top right redshift $z < 0.5$ panel gives the colour-colour space for the higher priority sample, while area "B" is for the lower priority sample.

We present the catalogue for the first 40 objects in ascending RA in Appendix A, with the entire catalogue to be published online with the publication of this paper. In the next Section we report in more detail on the properties of the high-redshift LRGs.

---

[1] "Qop" represents an integer redshift quality flag assigned by visual inspection of the galaxy spectrum and the redshift cross-correlation function. A value of 3 or greater represents a > 95% confidence that the redshift obtained from the spectrum is valid.

Field	COSMOS			COMBO-17 S11				2SLAQ d05			**Survey**
Selection	*gri*	$i < 20.5$	all	*gri*	$i < 20.5$	$z < 20.2$	all	*gri*	$i < 20.5$	all	**total**
Spectra Obtained	98	223	321	70	262	271	603	68	278	346	**1270**
$Q\text{op} \geq 3$	71	129	200	61	163	143	367	57	180	237	**804**
LRGs	67	89	156	55	119	80	254	50	127	177	**587**

Table 2. Redshift Statistics for the AAOmega LRG Pilot Run. These statistics are for the total exposure times as given in Table 1.

LRG Sample/ Field (Seeing)	d05 (1.″6)	S11 (1.″8)	COSMOS (2.″1)
gri $i < 19.8$ (2SLAQ)	88 ± 19	70 ± 22	64 ± 24
riz $19.8 < i < 20.5$	84 ± 13	60 ± 11	50 ± 9

Table 3. LRG percentage redshift completeness rates ($Q\text{op} \geq 3$) as estimated for $\simeq 80$ unfringed fibres between fibres 200-299 in a 1.67hr exposure (stars excluded). Better observing conditions (d05) yield completenesses consistent with 2SLAQ. Poorer observing conditions (S11 and COSMOS) yield lower completeness. The COSMOS data had average airmass 1.4 plus some cloud, as well as poorer seeing.

3.2 Redshift Completeness

The LRG redshift completeness statistics for each field can be calculated from Table 2 for the full, ≈ 4 hour, exposures and are given in Table 3 for a subset of data using 1.67 hour exposures. Our overall completeness was relatively low, compared to the 2SLAQ LRG Survey (Cannon et al. 2006), but one of the main reasons for this was due to the several technical issues associated with the new AAOmega instrument, which have since been corrected. When checks were made on the d05 field, we found that the redshift completeness rates for our *riz*, $19.8 < i_{\rm deV} < 20.5$ targets as estimated from ≈ 80 "unfringed" fibres were $90 \pm 9\%$ in ≈4 hour exposures, $84 \pm 13\%$ in 1.67 hour exposures in 1.″6 seeing. Thus, using the full number of sub-exposures we found no significant increase in redshift completeness compared to a 1.67 hour exposure, although this may still be due to conditions varying within the 3 hour exposure time. But our general conclusion is that with reasonable seeing and transparency, we achieve 85-90% redshift completeness in a 1.67 hour exposure. We show a selection of spectra from the subset of data taken in the d05 field in Figure 2. The top six panels show spetra of confirmed, $Q\text{op} \geq 3$ LRGs, with ranging magnitudes and redshifts, including a high redshift confirmed LRG at $z \approx 0.9$. The second bottom panel shows an unconfirmed, $Q\text{op} < 3$, spectrum, while the bottom spectrum is for a confirmed M-star. The improved AAOmega throughput and sky subtraction enables us to work further into the near-infrared, allowing us to probe higher redshifts. Note the prominent CaII H+K 4000Å break appears in all the confirmed spectra, as expected for an old stellar population.

We also confirmed that the exposure time needed to obtain reliable redshifts of LRGs selected in the same manner as the 2SLAQ survey (using a *gri*-band, $i < 19.8$ selection) was cut by a factor of ~ 4 from the old 2dF instrument. We note from Table 3 that at least in the more reasonable observing conditions for the d05 field that the completeness of the 1.67hr LRG sample is consistent with the high, 90%, completeness achieved for 2SLAQ LRGs.

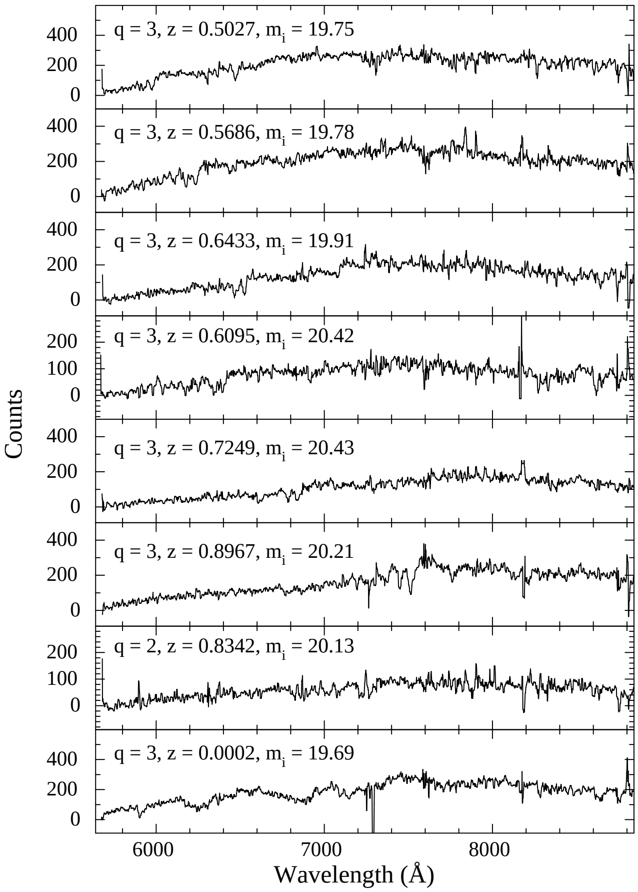

Figure 2. Examples of typical AAOmega spectra in 1.67hr exposures, from the *riz* selected, $19.8 < i < 20.5$ LRG sample. The top six panels show spetra of confirmed, $Q\text{op} \geq 3$ LRGs, with ranging magnitudes and redshifts. The second bottom panel shows an unconfirmed, $Q\text{op} < 3$, spectrum, while the bottom spectrum is for a confirmed stellar source.

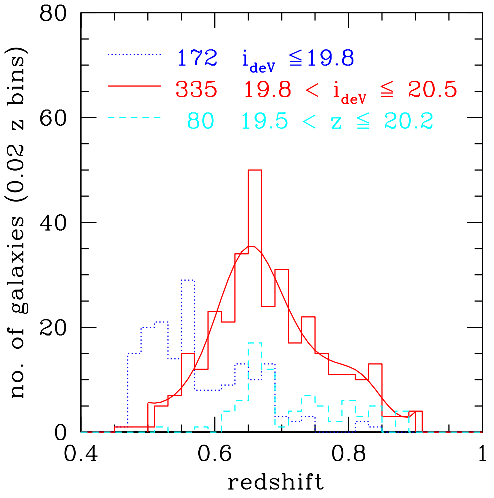

Figure 3. The $N(z)$ of $Qop \geq 3$ LRGs from the AAOmega LRG Pilot Run, showing that $0.5 \leq z \leq 0.9$ can be readily selected using SDSS *riz* photometry. The dotted (blue) histogram shows the distribution for the $i_{\rm deV} < 19.8$ *gri*-selection, while the solid (red) and the dashed (cyan) histograms show the *riz* selections with $19.8 < i_{\rm deV} < 20.5$ and $19.5 < z < 20.2$ respectively. We also plot the polynomial fit (red line) that is used to model the $N(z)$ distribution for the *riz*, $19.8 < i_{\rm deV} < 20.5$ selection in Section 4.2.

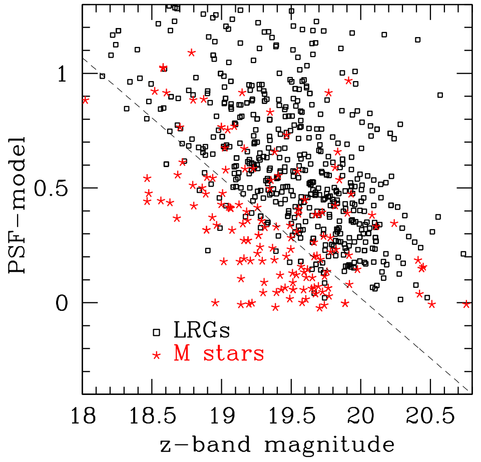

Figure 4. Star-Galaxy Separation using SDSS z-band magnitudes. All objects with $Qop \geq 3$ and $19.8 < i_{\rm deV} < 20.5$ are shown, with objects having stellar spectra plotted as (red) stars and objects having high-redshift LRG spectra plotted as (black) open squares. The ordinate gives the difference between the "PSF" and "Model" z-band magnitudes as given from the SDSS DR4 imaging.

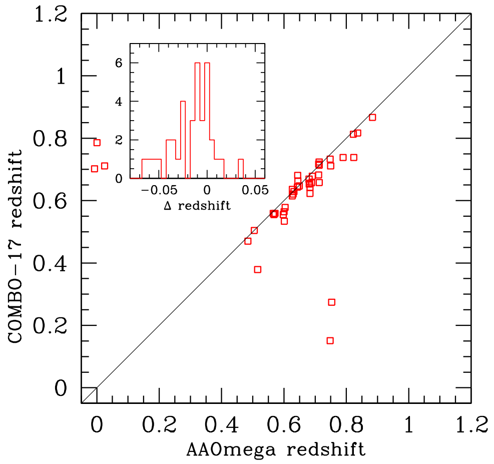

Figure 5. COMBO-17 photometric redshifts vs. AAOmega spectroscopic redshifts. The solid line is the 1:1 relation. The insert shows the histogram of $\Delta z = z_{\rm spec} - z_{\rm phot}$ for AAOmega and COMBO-17 redshifts respectively.

3.3 Redshift Distribution

The *raison d'être* of the AAOmega LRG Pilot run was to test if we could readily select $z \sim 0.7$ LRGs using single-epoch SDSS *riz*-photometry. As can be seen in Figure 3, where we plot the redshift distributions for confirmed $Qop \geq 3$ LRGs, this proved feasible. The mean redshift of our $19.8 < i_{\rm deV} < 20.5$ magnitude sample was $z = 0.681 \pm 0.005$, with a strong tail out to redshift $z = 0.8$ and indeed some objects at $z = 0.9$. We found that there was no major difference between the samples with different priorities (areas "A" and "B" in Figure 1). Also shown in Figure 1 are the *riz*-band colours for the objects with spectroscopically confirmed redshifts. When the magnitude limits applied were changed from $19.8 < i_{\rm deV} < 20.5$ to $19.5 < z < 20.2$, the mean redshift increased to $z = 0.698 \pm 0.015$. The mean redshift for our *gri*-band, $17.7 < i_{\rm deV} < 19.8$ selection was very comparable to the 2SLAQ LRG Survey at $z = 0.578 \pm 0.006$.

However, since we found that even though we were able to obtain LRG spectra for $z < 20.2$ objects from SDSS single-epoch imaging (and get the increase in redshift one might expect based on galaxy colours from evolutionary models), we find that the completeness of this sample dropped significantly and longer, ≥ 2 hours, exposures would be required in order to obtain $Qop \geq 3$ redshifts. This is not surprising considering that with a $z < 20.2$ magnitude limit, we are selecting objects with $i_{\rm deV}$ ~20.8 given a $(i - z)$ colour of ~0.6 (as seen in Fig. 1). Thus for the remainder of this analysis, and the eventual strategy for a large LRG-BAO Survey, we only consider objects with $19.8 < i_{\rm deV} < 20.5$.

As can be seen from Table 2, a significant fraction (27%) of our $Qop \geq 3$ objects were M-type stars. However, as shown in Figure 4, *a posteriori* checking shows that we can reject 40% of these stars using a star-galaxy separation in the z-band, rather than the standard SDSS separation performed in the r-band. The stellar contamination drops to 16%, with very few high-redshift galaxies being lost. Employing near-IR imaging data, specifically a $J - K > 1.3$ cut, would dramatically reduce the stellar contamination further, to the levels of a few percent.

3.4 2SLAQ, COMBO-17 and AAOmega Comparison

In Figure 5 we show a comparison between the spectroscopic redshifts we recorded from our AAOmega observations and those measured photometrically by the Classifying Objects

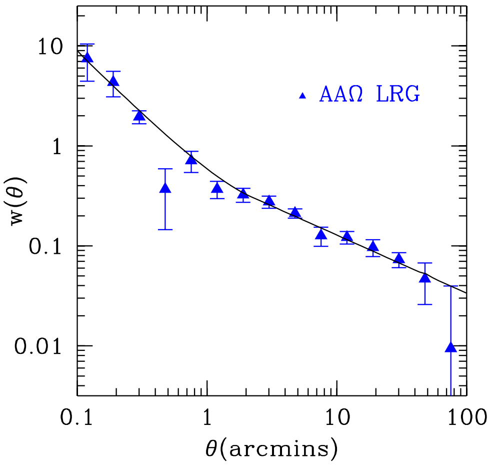

Figure 6. The AAOmega LRG Pilot angular correlation function, $w(\theta)$, is given by the solid (blue) triangles. 2 326 objects were used with magnitudes in the range $19.8 < i_{\rm deV} < 20.5$. The solid (black) line is a estimation of $w(\theta)$ given our redshift distribution and projecting using Limber's Formula, with the associated r_0 and γ jackknifed values given in Table 5.

by Medium-Band Observations (COMBO-17) survey (e.g. Wolf et al. 2003; Bell et al. 2004; Phleps et al. 2006). As can be seen, the 43 common photometric and spectroscopic redshifts match extremely well for the objects for which we have secure redshifts ($Q{\rm op} \geq 3$). There seems to be a slight trend for the photometric redshifts to underestimate the spectroscopic redshift. Why this is the case is not well understood. Excluding 5 "catastrophic failures", where $|\Delta z| \geq 0.2$, the average offset between the COMBO-17 photometric and AAOmega spectroscopic redshifts is $\overline{\Delta z} = 0.026 \pm 0.005$, in the sense that COMBO-17 redshifts are too small. There are 3 spectroscopically confirmed stars that COMBO-17 classified as redshift $z \sim 0.7$ galaxies.

We also compare the spectroscopic redshifts measured by AAOmega with those obtained in the 2SLAQ LRG Survey. We find, for the $Q{\rm op} \geq 3$ LRGs common in both, the mean $\Delta z = 8.4 \times 10^{-4}$ with the spread on the difference in redshifts being 1.24×10^{-3} i.e. 370 km s^{-1}. If the error is split evenly between the two surveys, then the error on AAOmega LRG redshifts is $\pm 370/\sqrt{2} = \pm 260$ km s^{-1}.

4 LRG CLUSTERING RESULTS

4.1 AAOmega LRG Angular Correlation Function, $w(\theta)$

Using the procedure described by Ross et al. (2007), the projected angular correlation function, $w(\theta)$, for the AAOmega LRG Pilot Survey is presented in Figure 6. The solid (blue) triangles are for the measurements made utilising the "Input Catalogue" from which objects were selected as potential high-redshift LRG candidates. Approximately 2 300 objects were used in this measurement from 6 fields that were observed by the 2SLAQ Survey, each π deg^2 in area. All these objects were potential targets having passed the *riz*-cuts discussed above. Field centres of the 6 fields are given in Table 4. It should also be noted that the star-galaxy separation discussed above was applied to this input sample. The error bars associated with the AAOmega LRG $w(\theta)$ measurement are *field-to-field* errors (see Ross et al. 2007) and do not take into account the fact that the clustering measurements are correlated and therefore, the errors on these points should only be regarded as indicative. When we come to calculate the errors on the fitted power-law parameters, defined in equation 7, we perform a jackknife analysis on our measurements in the attempt to take into account these covariances. This involves removing one field at a time from our sample and recomputing and refitting the angular correlation function, weighting by the number of DR pairs. As such, we present these jackknife errors for our measurements in Table 5.

Field Name	R.A. (J2000)	DEC (J2000)
2SLAQ c05	12h 38m 18s	-00 12 35
” c07	12h 47m 54s	-00 12 35
” d07	13h 31m 12s	-00 12 35
” e01	14h 34m 00s	-00 12 35
” e03	14h 42m 48s	-00 12 35
” c07	12h 47m 54s	-00 12 35

Table 4. Details of the 2dF fields that were used for the $w(\theta)$ measurements. Note, d05 was also used and details of this field are given in Table 1. All 6 fields were observed by the 2SLAQ Survey.

	2SLAQ LRG	AAOmega LRG
$r_{0,\rm ss}/\ h^{-1}$ Mpc	5.47±0.40	5.0±0.34
$\gamma_{\rm ss}$	2.16±0.07	2.28±0.04
$r_{0,\rm ls}/\ h^{-1}$ Mpc	8.0±0.8	10.2±0.7
$\gamma_{\rm ls}$	1.67±0.07	1.58±0.09

Table 5. The values of r_0 and γ for the 2SLAQ LRG Survey and AAOmega LRGs. Note that $r_b = 1.5\ \ h^{-1}$ Mpc for the 2SLAQ LRGs, while $r_b = 1.0\ \ h^{-1}$ Mpc for AAOmega LRGs. Also note that due to improved implementation of Limber's formula and more accurate binning, the values given here for r_0 and γ for the 2SLAQ LRG Survey from Limber's Formula, supersede those given by Ross et al. (2007).

A single power-law, of the form

$$\xi(r) = \left(\frac{r}{r_0}\right)^{-\gamma}, \tag{7}$$

where r_0 is the correlation length and γ the power-law slope, has traditionally been fitted for the 3-D correlation function for galaxies, ξ, and from which the relation,

$$w(\theta) = A\,\theta^{1-\gamma} \tag{8}$$

where A is amplitude, can be derived for the angular correlation function (e.g. Peebles, 1980). However, as was also found by Ross et al. (2007) for the 2SLAQ LRG $w(\theta)$, here we find that a double power-law model is required to fit the present measurement. Following that work, we use Limber's Formula (see Phillipps et al. 1978) to relate the 3-D correlation function to the our measured $w(\theta)$. A double power-law of the form

$$\xi(r) = \begin{cases} (r/r_{0,\mathrm{ss}})^{-\gamma_{\mathrm{ss}}} & r \leqslant r_{\mathrm{b}} \quad \text{and} \\ (r/r_{0,\mathrm{ls}})^{-\gamma_{\mathrm{ls}}} & r > r_{\mathrm{b}} \end{cases} \tag{9}$$

where ‘ss’ and ‘ls’ stand for small scales and large scales respectively, is assumed and calculated from Limber’s formula. The calculated values for r_0 and γ are given in Table 5, where we fit over the range $0.1' < \theta < 40.0'$ and note that $r_b = 1.5 \;\; h^{-1}$ Mpc for the 2SLAQ LRGs, while $r_b = 1.0 \;\; h^{-1}$ Mpc for AAOmega LRGs. We also note that due to improved implementation of Limber’s formula and more accurate binning, the values given here for r_0 and γ for the 2SLAQ LRG Survey from Limber’s Formula, supersede those given by Ross et al. (2007).

From Table 5, we can see that the $w(\theta)$ measurement for the AAOmega high-redshift data is comparable to the $z = 0.55$ data from the 2SLAQ LRG survey. At small scales, the observed AAOmega $w(\theta)$ slope is nearly equal to the 2SLAQ LRG measurement, while at large-scales, the AAOmega slope is slightly shallower than the 2SLAQ LRGs: $\gamma = 1.58 \pm 0.09$ for AAOmega compared to $\gamma = 1.67 \pm 0.07$ for 2SLAQ. However, given the associated errors, the two measurements are in very good agreement. We leave further analysis of the angular correlation function as reported here to Sawangwit et al. (2008, in prep.) who shall investigate the evidence for a double power-law feature in a much larger LRG sample.

Given the AAOmega LRG Pilot $N(z)$ (Figure 3) and using Limber’s Formula, the AAOmega $w(\theta)$ amplitude is expected to be 13% lower than the 2SLAQ LRG amplitude if there is no clustering evolution in comoving coordinates. Thus, in terms of the overall amplitude, this reinforces the impression given in Table 5 that AAOmega LRGs have a large-scale amplitude which is at least as high as the 2SLAQ LRGs. This finding is further backed up by measurements of the projected correlation function, $w_p(\sigma)$. We do not present our $w_p(\sigma)$ results here, but note that our best fitting (single) power-law to this data has an amplitude $r_0 = 9.0 \pm 0.9 \;\; h^{-1}$ Mpc and slope $\gamma = 1.73 \pm 0.08$ over the scales $1.0 < \sigma/ \;\; h^{-1}$ Mpc < 40.0 (where σ is the separation across the line-of-sight).

4.2 Redshift-space Correlation Function, $\xi(s)$

Using the spectroscopic redshift data we obtained in the COSMOS, S11 and d05 fields we now calculate the 3-D redshift-space correlation function, $\xi(s)$. We use the minimum variance estimator suggested by Landy & Szalay (1993) (proven to be an optimum estimator by Kerscher et al. (2000)) where

$$\xi(s) \;=\; 1 + \left(\frac{N_{rd}}{N}\right)^2 \frac{DD(s)}{RR(s)} - 2\left(\frac{N_{rd}}{N}\right)\frac{DR(s)}{RR(s)} \tag{10}$$

and DD, DR and RR are the number of data-data, data-random and random-random pairs at separation s respectively. We use bin widths of $\delta \log(s/ \;\; h^{-1}$ Mpc)=0.2 and the number density of random points was 20× that of the LRGs.

The random catalogue was made taking into account the angular incompleteness and the radial distribution of the objects in this Pilot. For each 2dF field we constructed a “quadrant bullseye” angular mask which consisted of 5 concentric rings divided into 4 quadrants. Using both the input catalogue and the 2dF instrument configuration positions, a completeness map was made in each of the 20 sectors. These completenesses then went into mimicking the angular selection function, from which a random catalogue was generated. Corrections for fibre collisions on small, $\lesssim 30$ arcseconds, scales were made by taking the ratio of the input catalogue $w(\theta)$ to the observed redshift catalogue $w(\theta)$, as described by Ross et al. (2007). The radial distribution was described by a high-order polynomial fit (shown as the red curve in Figure 3) to the AAOmega $N(z)$ for the 335 $19.8 < i < 20.5$ selected LRGs given in Figure 3. We also note that for ease of modelling, we truncate the polynomial fit (and thus the random radial distribution) at redshifts of $z \leq 0.50$ and $z \geq 0.90$.

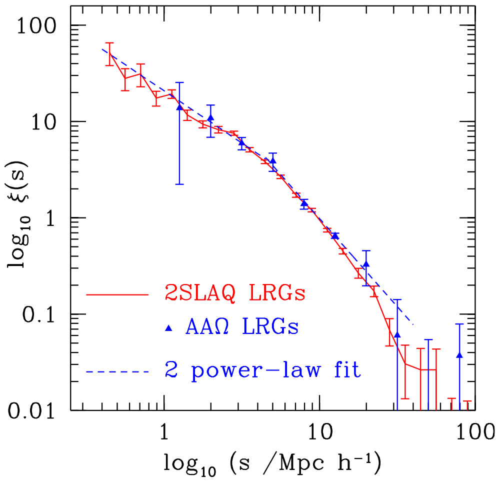

Figure 7. The AAOmega LRG Pilot Redshift-Space Correlation Function $\xi(s)$. The (blue) triangles are the measurements from the riz-selected $19.8 < i_{\mathrm{deV}} < 20.5$ sample, which yielded 335 $Qop \geq 3$ LRGs and the associated “Field-to-Field” errors. The dashed (red) line is the redshift-space correlation function from the 2SLAQ LRG Survey (Ross et al. 2007).

Figure 7 shows our estimate of the 3-D redshift-space correlation function, $\xi(s)$. Again, our error estimates are based on “field-to-field” errors. For $\xi(s)$, we use a double power-law model of the form given in equation 9, motivated by the fact that we expect the small-scale correlation function to be smoothed bt the effect of velocity dispersion (or “Fingers-of-God”) whereas at larger scales we expect the correlation function simply to be boosted due to infall, characterised by the parameter $\beta = \Omega^{0.6}/b$. We adopt the same procedure as for $w(\theta)$ and do a jackknife error analysis in order to estimate the errorbars on the best-fit double power-law model parameters. We find that, $s_{0,\mathrm{ss}} = 16.5 \pm 4.0 \;\; h^{-1}$ Mpc with $\gamma_{\mathrm{ss}} = 1.09 \pm 0.28$ on scales $s < 4.5 \;\; h^{-1}$ Mpc and $s_{0,\mathrm{ls}} = 9.9 \pm 0.7 \;\; h^{-1}$ Mpc with $\gamma_{\mathrm{ls}} = 1.83 \pm 0.35$ on scales $s > 4.5 \;\; h^{-1}$ Mpc. The clustering strength for the $19.8 < i < 20.5$, riz-selected AAOmega LRGs is again very comparable to the 2SLAQ LRG Survey, where $s_{\mathrm{ss}} = 17.3^{+2.5}_{-2.0} \;\; h^{-1}$ Mpc and $\gamma_{\mathrm{ss}} = 1.03 \pm 0.07$ on scales $s < 4.5 \;\; h^{-1}$ Mpc and $s_{\mathrm{ls}} = 9.40 \pm 0.19 \;\; h^{-1}$ Mpc and $\gamma_{\mathrm{ls}} = 2.02 \pm 0.07$ on scales $s > 4.5 \;\; h^{-1}$ Mpc.

Using the model of Kaiser (1987), we can find the pa-

Survey	mean redshift	$n/h^3\mathrm{Mpc}^{-3}$	Luminosity	h^{-1} Mpc	γ	Reference
AAOmega *riz* LRG	0.68	$\sim 2\times10^{-4}$	$\gtrsim 2L^*$	r_0 =10.2±0.7	1.58±0.09	1
				r_0 =9.0±0.9	1.73±0.08	2
				s_0 =9.9±0.7	1.83±0.35	3
2SLAQ LRG	0.55	$\sim 2\times10^{-4}$	$\gtrsim 2L^*$	s_0 =9.40±0.19	1.98±0.07	4, 5
				r_0 =7.45±0.35	1.72±0.06	4, 5
SDSS LRG	0.28	9.7×10^{-5}	$\geq 3L^*$	s_0 =11.85±0.23	1.91±0.07	6
				r_0 =9.80±0.20	1.94±0.02	6
MegaZ-LRG	0.63	5.6×10^{-5}	$\gtrsim 3L^*$	r_0 =9.3±0.3	1.94±0.02	7
COMBO-17	0.6	4×10^{-3}	$\sim L^*$	$r_0 = 5.39^{+0.30}_{-0.28}$	1.94±0.03	8
NDWFS	∼0.7	$\approx 1\times10^{-3}$	$> 1.6L^*$	r_0 =6.4±1.5	2.09±0.02	9, 10

Table 6. Values of s_0 and r_0 from the VST-AAΩ *ATLAS* LRG Pilot using the $w(\theta)$ measurement, the fit to $w_p(\sigma)$ and the $\xi(s)$ calculation with $s > 4.5$ h^{-1} Mpc. Values from the SDSS LRG Survey ($-23.2 < M_g < -21.2$), the 2SLAQ LRG Survey, MegaZ-LRG and the NDWFS are also given. Note that due to redshift-space distortions and other non-linear effects, r_0 will usually be smaller than s_0. (1) this work, from $w(\theta)$; (2) this work, from $w_p(\sigma)$; (3) this work, from $\xi(s)$; (4) Ross et al. (2007); (5) Wake et al. (2006); (6) Zehavi et al. (2005); (7) Blake et al. (2007); (8) Phleps et al. (2006); (9) White et al. (2007); (10) Brown et al. (2008).

rameter β via

$$\xi(s) = \xi(r)\left(1 + \frac{2}{3}\beta + \frac{1}{5}\beta^2\right). \tag{11}$$

We use our power-law fit for $\xi(r)$ and our large-scale power-law fit to $\xi(s)$ and find that the ratio $\xi(s)/\xi(r) = 1.3 \pm 0.3$ corresponding to a value of $\beta \simeq 0.4$ at a scale of 8 h^{-1} Mpc. This is not inconsistent with the value $\beta = 0.45 \pm 0.05$ found for the 2SLAQ LRGs, though clearly the errorbar is large. Nevertheless, for a reasonable value of β, our values of $s_0 = 9.9 \pm 0.7$ h^{-1} Mpc and $r_0 = 9.0 \pm 0.9$ h^{-1} Mpc appear consistent. These high clustering amplitudes clearly suggest that at $z \simeq 0.7$, LRGs remain very strongly clustered.

5 DISCUSSION

5.1 Clustering amplitudes and bias of LRGs at $z \simeq 0.7$

Now that we have calculated the AAOmega LRG angular, projected, and 3-D redshift-space correlation functions we can use these measurements to infer the physical properties of LRGs. Before proceeding to determine typical LRG halo masses using simple 'halo occupation' models, we first compare the clustering amplitudes and biases of the AAOmega LRGs with other LRG results, taking into account the different redshift and luminosity ranges. For reference, a summary of results of space densities, luminosity limits and clustering amplitudes from the AAOmega LRG, 2SLAQ LRG, SDSS LRG, MegaZ-LRG, COMBO-17 and NDWFS surveys, is given in Table 6. We note, however, that direct comparisons between clustering results from surveys with different e.g. magnitude and colour selections can be complex.

We have found that a 2-power law fit is consistent with AAOmega $w(\theta)$ data. The slopes of the AAOmega power-law fits are both less than those for the 2SLAQ LRG Survey (Ross et al. 2007). This could be due to evolution with redshift but the errors on the AAOmega $w(\theta)$ are too large for this difference to be significant. Certainly the large scale results from $\xi(s)$ are perfectly consistent with the two surveys having the same large-scale slope and amplitude (see Fig. 7).

We further note that from both the fitting of Limber's formula to $w(\theta)$ and describing $w_p(\sigma)$ with a simple power-law, we find the real-space clustering amplitude of AAOmega LRGs is consistent with that from the SDSS LRG Survey (Zehavi et al. 2005), though our errors are large. Using our r_0 estimate from $w_p(\sigma)$, (which has the smaller error and more closely matched power-law slope), we note that AAOmega LRGs have a slightly lower clustering amplitude than SDSS LRGs, $r_0 = 9.0 \pm 0.9$ h^{-1} Mpc versus $r_0 = 9.80 \pm 0.20$ h^{-1} Mpc respectively. However, this is not surprising since SDSS LRGs have a redder colour selection and higher luminosity, and this may explain their higher clustering amplitude.

To calculate the value of the linear bias, b, for the AAOmega LRGs, we use the integrated correlation function (Croom et al. 2005; da Ângela et al. 2008),

$$\xi_{20}(r) = \frac{3}{r_{\rm max}^3}\int_0^{r_{\rm max}} \xi(r) r^2 dr \tag{12}$$

where we set $r_{\rm max} = 20$ h^{-1} Mpc since this is a large enough scale for linear theory to apply and also, due to the r^2 weighting, small-scale redshift-space distortions should be negligible. We first calculate the integrated mass correlation function using the $\sigma_8 = 0.84$ normalised ΛCDM model for $P(k)$ from Smith et al. (2003) with $\Omega_{\rm m}(z=0) = 0.27$. We find $\xi_{20}^{\rm mass} = 0.12$ at the 2SLAQ LRG mean redshift $z = 0.55$ and $\xi_{20}^{\rm mass} = 0.11$ at the AAOmega LRG mean redshift $z \simeq 0.70$.

We then calculate the integrated galaxy correlation function assuming $r_0 = 7.45 \pm 0.35$ h^{-1} Mpc and hold γ fixed at 1.72 for the 2SLAQ LRGs Ross et al. (2007) and $r_0 = 9.03 \pm 0.93$ h^{-1} Mpc, $\gamma = 1.73$ for AAOmega LRGs. We find that $b_{\rm 2SLAQ} = 1.90 \pm 0.08$ and $b_{\rm AAOmega} = 2.35 \pm 0.22$, where $b = (\xi_{20}/\xi_{\rm mass,20})^{1/2}$. The value of $b_{\rm 2SLAQ} = 1.90 \pm 0.08$ is higher, but consistent with that found by Ross et al. (2007), who found $b_{\rm 2SLAQ} = 1.66 \pm 0.35$, from z-space distortion analysis, and we suggest the error presented here may be an underestimate since γ is being held at a fixed value. The value of $b_{\rm AAOmega} = 2.35 \pm 0.22$ is higher than for the 2SLAQ LRGs, but the large error on the AAOmega result means there may be no inconsistency here. However, our value of $b_{\rm AAOmega} = 2.35 \pm 0.22$ is even higher than that reported for the SDSS LRGs at lower redshifts, who report values of $b \approx 1.8$ (Padmanabhan et al. 2007). Although an increase in bias is expected due to the higher redshift of the AAOmega sample, the effect is larger than predicted especially taking into account the bluer AAOmega selection. But again the large error on $b_{\rm AAOmega}$ renders this difference statistically insignificant.

To see what sort of consistency with 2SLAQ might be expected, we can predict the value of b at redshift $z = 0.7$ by utilising the values measured by 2SLAQ at lower redshift, $b(z = 0.55) = 1.66 \pm 0.35$, and the bias evolution model given by Fry (1996); Croom & Shanks (1996),

$$b(z) = 1 + [b(0) - 1]G(\Omega_{\rm m}(0), \Omega_\Lambda(0), z). \quad (13)$$

Here, $G(\Omega_{\rm m}(0), \Omega_\Lambda(0), z)$ is the linear growth rate of the density perturbations (Peebles 1980, 1984; Carroll et al. 1992). There are many other bias models, but here we are following Ross et al. (2007, and references therein) by making the simple assumptions that galaxies formed at early times and their subsequent clustering is governed purely by their discrete motion within the gravitational potential produced by the matter density perturbations. This model would be appropriate, for example, in a "high-peaks" biasing scenario where early-type galaxies formed at a single redshift and their co-moving space density then remained constant to the present day.

Thus, assuming a growth rate of $G(0.3, 0.7, z)$, to relate $\xi_{\rm mm}(z = 0.55)$ to $\xi_{\rm mm}(z = 0.7)$, we therefore expect $\xi_{\rm gg}(z = 0.7) = 0.94\,\xi_{\rm gg}(z = 0.55)$ from this model. From Table 6 the r_0 values between 2SLAQ and AAOmega LRGs are consistent, although the errors on the AAOmega r_0 measurement are big. But the errors on $\xi(s)$ are smaller, and even here, the s_0 values agree to within the errors (see also Figure 7). The consistency of the clustering results is expected, since the 0.7 magnitudes deeper $19.8 < i_{deV} < 20.5$ selection was based on experience from the 2SLAQ LRG Survey and primarily designed to select similarly highly-biased red galaxies at redshift $z \simeq 0.7$. We conclude that the LRG correlation function amplitudes are similar at redshifts $z \approx 0.55$ and $z \approx 0.7$ and that there is still no inconsistency with the simple bias model where the comoving density of LRGs are assumed to be constant with redshift.

5.2 Predictions of halo occupation models

An alternative approach to interpreting our measured level of clustering is to use the halo occupation model, in which the galaxy field is taken to be a superposition of contributions from dark-matter haloes, weighted by the number of galaxies per halo, $N(M)$. This methodology is commonly reffered to as a 'halo occupation distribution', or HOD, model and was used recently by Phleps et al. (2006) to model the projected correlations in the COMBO-17 survey. We apply exactly the same method as described in that paper to model our AAOmega data, specifically for our $w_p(\sigma)$ measurement. Again we adopt a standard matter power spectrum, with $\Omega_m = 0.3$, $\Omega_b = 0.045$, $h = 0.73$, $\sigma_8 = 0.85$, and a scalar spectral index of 0.97. The occupation model is the simplest possible: $N(M) = (M/M_{\rm min})^\alpha$ for $M > M_{\rm min}$. These two free parameters are reduced to one if the model is also required to match the number density of LRGs, which is approximately $0.0002\,h^3\,{\rm Mpc}^{-3}$.

Realistic occupation models will be more complicated than this simple power-law form, but Phleps et al. argue that the results can be expressed quite robustly in terms of an effective halo mass – i.e. the average halo mass weighted by the number of galaxies. For our current data, the occupation parameters that best match the clustering measurements are $\alpha \simeq 0.7$ and $M_{\rm min} \simeq 2\times10^{13}h^{-1}M_\odot$. These imply an average halo mass for the AAOmega LRGs at $z \simeq 0.7$ of $M_{\rm eff} \simeq 7 \times 10^{13}h^{-1}M_\odot$. Reasonably enough for particularly rare and luminous galaxies such as those studied here, this mass is somewhat larger than the figure found by Phleps et al. for the COMBO-17 red-sequence galaxies at $z \simeq 0.6$, which was $M_{\rm eff} \simeq 1.6 \times 10^{13}h^{-1}M_\odot$, using the same methodology. Our AAOmega figure for $M_{\rm eff}$ is in fact almost identical to the average mass deduced for $z = 0$ red-sequence galaxies in SDSS. Of course, this coincidence does not imply any direct correspondence between these populations: the haloes that host our $z \simeq 0.7$ LRGs may have become much more massive by the present.

Blake et al. (2007) calculate the LRG angular correlation function using the "MegaZ-LRG" galaxy database, which is a large photometric-redshift catalogue of luminous red galaxies extracted from the SDSS imaging data (Collister et al. 2007). They then successfully model the observations using a HOD model with a "central" galaxy contribution and a "satellite" galaxy component. Noting that comparison of results are strongly dependent on the overall normalization of the power spectrum, σ_8, we compare our effective mass value for the AAOmega LRGs at $z \simeq 0.7$ of $M_{\rm eff} \simeq 7 \times 10^{13}h^{-1}M_\odot$ ($\sigma_8 = 0.85$) to that of the highest redshift bin by Blake et al. (2007) of $0.6 < z < 0.65$ and find their $M_{\rm eff} = 9.5 \pm 0.7 \times 10^{13}h^{-1}M_\odot$ ($\sigma_8 = 0.8$) to be $\sim 30\%$ larger than our effective mass estimate. However, after further analysis these authors have revised their $M_{\rm eff}$ estimates (C. Blake priv. comm) and we await comparisons to their new results.

White et al. (2007) and Brown et al. (2008) have used data from the 9 deg^2 Boötes field, which has been imaged in the optical and infrared as part of the NOAO Deep Wide Field Survey (NDWFS; Jannuzi & Dey 1999; Brown et al. 2008), and by the *Spitzer* IRAC Shallow Survey (Eisenhardt et al. 2004). White et al. (2007) use the clustering of luminous red galaxies from these observations (and N-body simulations) to argue that about $\frac{1}{3}$ of the most luminous satellite galaxies appear to undergo merging or disruption within massive halos between $z \simeq 0.9$ and 0.5. Brown et al. (2008) report a correlation length of $r_0 = 6.4\pm1.5\ \ h^{-1}$ Mpc for their brightest red galaxy sample, $M_B - 5\log h < -21.0$ (corresponding to $L > 1.6L^*$ galaxies), across the redshift range $0.6 < z < 0.8$. These authors also calculate the bias for this sample to be $b = 2.15 \pm 0.08$. Thus, although the NDWFS LRGs and AAOmega LRGs have different selections (e.g. different magnitude and redshift limits), evidence from both surveys suggest that redshift $z = 0.7$ LRGs are highly-biased objects and thus extremely well-suited to LSS studies.

5.3 LRGs versus ELGs

One of the key questions that the AAOmega LRG Pilot Survey wanted to address, was whether a "blue" or a "red" galaxy survey be the more advantageous when pursuing BAOs at high redshift. In the previous sections, we have presented the $N(z)$ and clustering amplitudes for $\bar{z} = 0.68$ Luminous Red Galaxies. As such, our 'Pilot' observations

Scale	**ELG**		**LRG**		**$V_{\rm eff}$ LRG / $V_{\rm eff}$ ELG**	
$k/h\,{\rm Mpc}^{-1}$	$P/h^{-3}\,{\rm Mpc}^3$	$V_{\rm eff}/h^{-3}{\rm Gpc}^3$	$P/h^{-3}\,{\rm Mpc}^3$	$V_{\rm eff}/h^{-3}{\rm Gpc}^3$	167/123 nts.	Equal no. nts.
0.02	$6.7{\times}10^4$	1.1	1×10^5	1.9	1.7	1.3
0.05	$2.7{\times}10^4$	0.82	4×10^4	1.4	1.7	1.3
0.15	$6.7{\times}10^4$	0.42	1×10^4	0.61	1.5	1.1

Table 7. A comparison between the effective volumes probed by two AAOmega-based BAO Surveys, one using Luminous Red Galaxies (LRGs) and one using Emission Line Galaxies (ELGs). We assume a factor of 1.5 between the clustering amplitudes of LRGs and ELGs. The second last column is an effective volume ratio for 360 000 LRGs over 3000 deg^2 with 70-90% completeness (1.5hr exposures per field) versus 400 000 ELGs over 1000 deg^2 (1hr exposure) with 80% completeness both assuming 9hr nights. This gives a total observing requirement of 167 nights for LRGs and 123 nights for ELGs, implying the effective volume ratios given in the sixth column. The last column is the effective volume ratio assuming the same number of nights for both projects.

suggest, a VST-AAΩ *ATLAS* spectroscopic redshift survey strategy to pursue BAOs with AAOmega LRGs might consist of ≈1.5 hour exposures with

- $\simeq 100$ fibres placed on *gri*-selected $i < 19.8$ LRGs with $z \simeq 0.55$ and
- $\simeq 260$ fibres placed on *riz*-selected $19.8 < i < 20.5$ LRGs with $z \simeq 0.7$

in order to obtain 360 000 LRGs over 3000deg^2 which will give an $\sim 4\times$ bigger effective volume than the original SDSS LRG Survey of 45,000 LRGs (Eisenstein et al. 2005). We shall compare this strategy, with an alternate "Emission Line Galaxy" (ELG) survey, in the remainder of this section.

Glazebrook et al. (2007) select "blue" emission line galaxies (ELGs) using SDSS and *GALEX* Far ultra-violet (FUV) and Near ultra-violet (NUV) imaging (Martin et al. 2005), for the *WiggleZ* BAO Dark Energy Survey. By using the reported $N(z)$ in Glazebrook et al. (2007, Figure 2) which has an average redshift of $z \simeq 0.6 \pm 0.2$ as well as their estimate of the clustering amplitude, we can make a comparison with our data. The clustering amplitude reported initially by Glazebrook et al. (2007) is $s_0 = 3.81 \pm 0.20$ h^{-1} Mpc (their Figure 3). However, it has recently been suggested that an improved *GALEX* ELG Selection for *WiggleZ* may give a higher ELG clustering amplitude of $r_0 \approx 6$ h^{-1} Mpc (C. Blake priv. comm.) leading to $s_0 \approx 9$ h^{-1} Mpc assuming $\beta(z \approx 0.7) = 0.8$ and applying equation 11. We use this higher value, along with the appropriate redshift distributions for ELGs (truncated at redshift $z < 0.5$ due to the *WiggleZ* Survey plans to focus on $z > 0.5$ galaxies only) and LRGs (from our Fig. 3) and assuming that bias is scale independent.

We can calculate the effective volume surveyed using (e.g. Tegmark et al. 2006):

$$V_{\rm eff} = \int \left[\frac{n(\mathbf{r})\, P_g(k)}{1 + n(\mathbf{r})\, P_g(k)} \right]^2 dV. \tag{14}$$

where $n(\mathbf{r})$ is the comoving number density of the sample, (in units of h^3 Mpc^{-3}) and $P_g(k)$ is the value of the galaxy Power Spectrum at wavenumber k (with units of h Mpc^{-1}). For the LRG Survey we assume ≈360 000 redshifts are required with 100 fibres targeted on $i < 19.8$, redshift $z \simeq 0.55$ 2SLAQ LRGs with 90% completeness, to account for 5% redshift incompleteness and 5% stellar contamination, and 260 fibres on $19.8 < i < 20.5$ $z \simeq 0.7$ AAOmega LRGs with 70% completeness (15% redshift incompleteness and 15% stellar contamination). For the ELG Survey, we assume 360 fibres targeted on ELGs, as described above, with 80% redshift completeness. Therefore, we see that *(i)* a 167 night LRG survey would have ≈ 1.7× the effective volume of a 123 night ELG survey as envisaged by Glazebrook et al. and *(ii)* for equal telescope time, an LRG survey will sample ≈ 1.3× the effective volume of an ELG Survey (see Table 6). The above results are approximately in line with those of Parkinson et al. (2007) who present "Figures of Merit" (FoM) calculations to judge the optimality of different survey designs for future galaxy redshift-based BAO experiments.

6 CONCLUSIONS

We have reported on the AAOmega-AAT LRG Pilot observing run to establish the feasibility of a large spectroscopic survey aimed at detecting BAO and present some of the first results from the new AAOmega instrument. We have confirmed that AAOmega has a factor of approximately four in improved throughput in its red (> 5700Å) arm as compared to the old 2dF spectrographs. Utilising this new sensitivity, we observed Luminous Red Galaxies (LRGs) selected using single epoch SDSS *riz*-photometry in 3 fields including the COSMOS field, the COMBO-17 S11 field and the previously observed 2SLAQ Survey field, d05. Our main conclusions are:

- We detect 1270 objects in three fields, of which 587 are confirmed high-redshift LRGs. The mean redshift for each selection was $\bar{z} = 0.578 \pm 0.006$ from the *gri*-band selection with $17.5 < i_{\rm deV} < 20.5$, $\bar{z} = 0.681 \pm 0.005$ from the *riz*-band selection with $19.8 < i_{\rm deV} < 20.5$ and $\bar{z} = 0.698 \pm 0.015$ from the *riz*-band selection with $19.5 < z < 20.2$. At $i < 20.5$, 84% redshift completeness for LRGs was achieved in 1.67hr exposures in reasonable conditions.
- We have compared our AAOmega spectroscopic redshifts to spectroscopic and photometric redshifts obtained by the 2SLAQ LRG Survey and COMBO-17 respectively. We find excellent agreement with the 2SLAQ spectroscopic redshifts, but a suggestion that there is a systematic tendency of the photometric redshifts to underestimate the spectroscopic redshifts by $\overline{\Delta z} = 0.026 \pm 0.005$.
- We find that a simple power-law model, for $w_p(\sigma)$, gives a best fit value of $r_0 = 9.03 \pm 0.93$ for our $\bar{z} = 0.68$ LRG

sample, compared to $r_0 = 9.80 \pm 0.20$ for the $-21.2 < M_r < -23.2$ SDSS LRG sample and $r_0 = 7.30 \pm 0.34$ for the $\bar{z} = 0.55$ 2SLAQ LRG sample. This confirms that high-redshift luminous red galaxies are very good large-scale structure tracers, similar to their lower redshift counterparts (Zehavi et al. 2005; Eisenstein et al. 2005; Ross et al. 2007).

- We also find that, taking into account the large errors on the AAOmega LRG r_0 measurement, there is no inconsistency with the simple bias model where the comoving density of LRGs are assumed to be constant with redshift.
- Finally, this Pilot project shows that a large-scale AAOmega spectroscopic survey of highly biased $z \sim 0.7$ 360 000 LRGs over 3000deg^2, remains a very promising and competitive route in order to measure the baryon acoustic oscillations and use this scale-length to investigate the potential evolution of the equation of state parameter, w.

ACKNOWLEDGEMENT

We thank C. Wolf for supplying the COMBO-17 photometric redshift catalogue data in the S11 field and U. Sawangwit for providing the Bruzual and Charlot models. We also thank R. Angulo, C.M. Baugh and R.M. Bielby for useful discussion. This work was supported by a PPARC PhD Studentship and by National Science Foundation grant AST-0607634 (N.P.R.) We warmly thank all the present and former staff of the Anglo-Australian Observatory for their work in building and operating the AAOmega facility. The AAOmega LRG Pilot is based on observations made with the Anglo-Australian Telescope and with the SDSS. Funding for the creation and distribution of the SDSS Archive has been provided by the Alfred P. Sloan Foundation, the Participating Institutions, the National Aeronautics and Space Administration, the National Science Foundation, the U.S. Department of Energy, the Japanese Monbukagakusho, and the Max Planck Society. The SDSS Web site is `http://www.sdss.org/`. The SDSS is managed by the Astrophysical Research Consortium (ARC) for the Participating Institutions. The Participating Institutions are The University of Chicago, Fermilab, the Institute for Advanced Study, the Japan Participation Group, The Johns Hopkins University, the Korean Scientist Group, Los Alamos National Laboratory, the Max-Planck-Institute for Astronomy (MPIA), the Max-Planck-Institute for Astrophysics (MPA), New Mexico State University, University of Pittsburgh, University of Portsmouth, Princeton University, the United States Naval Observatory, and the University of Washington.

REFERENCES

Adelman-McCarthy, J. K., et al., 2006, ApJS, 162, 38
Angulo, R. E., Baugh, C. M., Frenk, C. S., & Lacey, C. G. 2008, MNRAS, 383, 755
Bailey, J. A., Heald, R., Croom, S, M., 2005, The 2DFDR Data Reduction System Users Manual, AAO, `http://www.aao.gov.au/AAO/2dF/manual.html`
Baugh C. M., Lacey C. G., Frenk C. S., Granato G. L., Silva L., Bressan A., Benson A. J., Cole S., 2005, MNRAS, 356, 1191
Bell E. F., et al., 2004, ApJ Lett., 600, L11
Brown M. J. I., et al., 2008, ApJ submitted
Blake, C., Collister, A., & Lahav, O. 2007, ArXiv e-prints, 704, arXiv:0704.3377
Blake C. & Glazebrook K., 2003, ApJ, 594, 665
Bruzual G., Charlot S., 2003, MNRAS, 344, 1000
Cannon R., et al., 2006, MNRAS, 372, 425
Carroll S. M., Press W. H., Turner E. L., 1992, ARA&A, 30, 499
Cole S., et al., 2005, MNRAS, 362, 505
Colless M., et al., 2001, MNRAS, 328, 1039
Collister, A., et al. 2007, MNRAS, 375, 68
Croom, S. M., et al. 2005, MNRAS, 356, 415
Croom S. M. & Shanks T., 1996, MNRAS, 281, 893
da Ângela J., et al., 2008, MNRAS, 383, 565
Eisenhardt, P. R., et al., 2004, ApJS, 154, 48
Eisenstein D. J., et al., 2001, AJ, 122, 2267
Eisenstein D. J., et al., 2003, ApJ, 585, 694
Eisenstein D. J., et al., 2005, ApJ, 633, 560
Eisenstein, D. J., Seo, H.-J. & White, M., 2007, ApJ, 664, 660
Eisenstein D. J., & Hu W., 1998, ApJ, 496, 605
Fry J. N., 1996, ApJ Lett., 461, L65
Fukugita M., Ichikawa T., Gunn J. E., Doi M., Shimasaku K., & Schneider D. P., 1996, AJ, 111, 1748
Glazebrook K., et al., 2007, astro-ph/0701876
Gunn J. E., et al., 2006, AJ, 131, 2332
Hatton S., & Cole S., 1998, MNRAS, 296, 10
Hawkins E., et al., 2003, MNRAS, 346, 78
Hütsi, G., 2006, Astron. & Astrophys., 449, 891
Jannuzi, B. T., & Dey, A. 1999, Photometric Redshifts and the Detection of High Redshift Galaxies, 191, 111
Kaiser N., 1987, MNRAS, 227, 1
Kerscher, M., Szapudi, I., & Szalay, A. S., 2000, ApJ Lett., 535, L13
Landy S. D., Szalay A. S., 1993, ApJ, 412, 64
Lawrence, A., et al., 2007, MNRAS, 379, 1599
Loh Y.-S., Strauss M. A., 2006, MNRAS, 366, 373
Martin D. C., et al., 2005, ApJ Lett., 619, L1
Martínez, V. J., & Saar, E. 2002, Statistics of the Galaxy Distribution, Published by Chapman & Hall/CRC, Boca Raton, ISBN: 1584880848
Meiksin, A., White, M., & Peacock, J. A. 1999, MNRAS, 304, 851
Padmanabhan N., et al., 2007, MNRAS, 378, 852
Parkinson D., Blake C., Kunz M., Bassett B. A., Nichol R. C., & Glazebrook K., 2007, MNRAS, 377, 185
Peebles P. J. E., 1980, The Large-Scale Structure of the Universe. Princeton University Press.
Peebles P. J. E., 1984, ApJ, 284, 439
Percival W. J., 2007, ApJ, 657, 51
Percival W. J., 2007, ApJ, 657, 645
Phillipps S., Fong R., Fall S. M., Ellis R. S. & MacGillivray H. T., 1978, MNRAS, 182, 673
Phleps S., Peacock J. A., Meisenheimer K., & Wolf C., 2006, Astron. & Astrophys., 457, 145
Press W. H., Teukolsky S. A., Vetterling W. T., & Flannery B. P., 1992, Numerical Recipes in FORTRAN: The Art of Scientific Computing. Cambridge University Press.
Ross N. P., et al., 2007, MNRAS, 381, 573
Salpeter E. E., 1955, ApJ, 121, 161

Saunders W., Rowan-Robinson M., & Lawrence A., 1992, MNRAS, 258, 134
Scoccimarro R., 2004, Phys. Rev. D, 70, 083007
Scoville N., et al., 2007, ApJS, 172, 1
Seo H.-J., & Eisenstein D. J., 2003, ApJ, 598, 720
Seo H.-J., & Eisenstein D. J., 2005, ApJ, 633, 575
Seo, H.-J., & Eisenstein, D. J. 2007, ApJ, 665, 14
Sharp R., et al., 2006, Proceedings of the SPIE, 6269,
Smith, R. E., et al. 2003, MNRAS, 341, 1311
Stoughton C., et al., 2002, AJ, 123, 485
Tegmark M., et al., 2006, Phys. Rev. D, 74, 123507
Wake D. A., et al., 2006, MNRAS, 372, 537
White, M., Zheng, Z., Brown, M. J. I., Dey, A., & Jannuzi, B. T. 2007, ApJ Lett., 655, L69
Wolf, C., Meisenheimer, K., Rix, H.-W., Borch, A., Dye, S., & Kleinheinrich, M., 2003, Astron. & Astrophys., 401, 73
Yamamoto K., Bassett B. A., Nichol R. C., Suto Y., Yahata K., 2006, Phys. Rev. D, 74, 063525
York D. G., et al., 2000, AJ, 120, 1579
Zehavi I., et al., 2005, ApJ, 621, 22

APPENDIX A: THE AAOMEGA LRG PILOT DATA

In Table A1 we present properties of the first 40 objects from the AAOmega Pilot Catalogue in Right Ascension order. The full dataset is published in its entirety in the electronic edition of the *Monthly Notices of the Royal Astronomical Society*.

Object ID[1]	α	δ	r-fibre [2]	T[3]	X-cor[4]	redshift	Qop	Field	u	g	r	i	z	$u_{\rm err}$	$g_{\rm err}$	$r_{\rm err}$	$i_{\rm err}$	$z_{\rm err}$
J095618.80+021623.2	149.07835	2.27312	20.14	1	6.34	0.6716	3	cos	23.6300	23.2400	21.7760	20.5030	19.8820	1.0310	0.2800	0.1210	0.0730	0.1770
J095634.36+015804.9	149.14317	1.96803	19.48	1	5.51	0.5510	3	cos	22.9990	22.0510	20.5420	19.4830	18.8840	0.7910	0.1420	0.0600	0.0410	0.0910
J095637.67+015254.7	149.15698	1.88187	20.10	1	3.47	0.5686	3	cos	24.3040	22.6720	21.4140	20.2050	19.8920	1.2250	0.1650	0.0890	0.0530	0.1490
J095639.34+021709.2	149.16393	2.28590	20.27	1	4.91	0.5457	3	cos	23.4230	23.1880	21.2570	20.2020	19.4730	1.1030	0.3510	0.1080	0.0720	0.1670
J095647.19+022325.2	149.19666	2.39035	19.73	1	5.57	0.5357	3	cos	25.4570	22.6930	20.7560	19.7260	19.7420	1.4010	0.2240	0.0710	0.0480	0.2130
J095649.24+021838.6	149.20519	2.31073	19.10	1	5.00	0.4806	3	cos	23.1220	21.7150	20.0390	19.1010	18.6840	0.8970	0.0990	0.0400	0.0290	0.0840
J095649.42+023355.3	149.20592	2.56537	19.93	2	3.30	0.9373	1	cos	21.5160	26.4460	21.3550	19.9320	19.3920	0.5760	1.6790	0.3160	0.1550	0.3360
J095649.86+020743.4	149.20776	2.12875	20.33	2	3.06	0.9444	2	cos	22.5640	23.1070	21.2320	20.3290	19.4470	0.5350	0.2970	0.0920	0.0670	0.1380
J095654.01+020225.0	149.22507	2.04028	20.41	1	6.03	0.6589	3	cos	23.1800	23.3520	21.9510	20.6320	20.0930	0.6970	0.2810	0.1320	0.0660	0.1870
J095702.89+024208.9	149.26208	2.70250	19.78	1	3.49	0.6792	4	cos	22.2880	21.7660	20.7220	19.7830	19.4340	0.3290	0.0900	0.0620	0.0470	0.1110
J095702.94+014853.3	149.26228	1.81481	20.29	1	2.98	0.7001	2	cos	24.7150	24.6660	22.2380	20.9450	20.6940	1.5400	0.8110	0.2040	0.1040	0.3320
J095703.84+015133.8	149.26600	1.85940	20.48	1	3.90	0.6355	3	cos	24.8210	22.9440	22.1000	20.8850	20.5140	1.2970	0.2120	0.1840	0.1030	0.2660
J095705.34+024238.2	149.27227	2.71061	20.46	3	3.27	0.0225	2	cos	23.4330	22.8750	22.5620	20.7060	20.4770	1.0860	0.3040	0.4100	0.1370	0.3660
J095705.95+021834.5	149.27483	2.30959	20.14	1	3.47	0.8355	2	cos	26.6360	24.5210	22.0400	20.1440	19.9200	0.8420	1.3890	0.3450	0.1050	0.3750
J095707.64+023955.2	149.28184	2.66533	19.95	3	7.88	0.0010	3	cos	24.5950	22.7660	21.6200	19.9550	19.3470	1.5510	0.2390	0.1550	0.0610	0.1150
J095708.35+014747.4	149.28483	1.79652	20.16	2	2.75	0.9454	2	cos	22.0610	22.9460	21.9640	20.1640	19.5390	1.2060	1.0070	0.6780	0.2210	0.5190
J095709.77+020506.6	149.29071	2.08519	20.35	3	4.97	0.0004	3	cos	22.9240	22.7870	21.4720	20.2040	19.7110	0.6020	0.1890	0.0930	0.0510	0.1410
J095712.04+015554.2	149.30018	1.93172	20.01	1	3.40	0.4818	3	cos	25.9540	22.1380	21.0040	20.0080	19.8880	0.7680	0.1210	0.0780	0.0530	0.1750
J095712.53+021202.8	149.30223	2.20079	20.26	1	3.43	0.8407	3	cos	22.0080	21.9630	21.7840	20.5500	20.0970	0.4650	0.1580	0.2190	0.1200	0.3680
J095713.39+015241.0	149.30579	1.87807	19.82	1	6.31	0.6434	3	cos	24.6310	22.6460	20.9660	19.8160	19.2770	1.5990	0.2100	0.0840	0.0500	0.1140
J095713.89+015210.8	149.30789	1.86967	20.14	3	2.44	0.0449	2	cos	22.7680	22.4500	21.5830	20.1400	19.9110	1.0200	0.3280	0.2630	0.1210	0.3740
J095719.14+020154.6	149.32975	2.03184	19.85	1	3.78	0.5553	3	cos	23.0910	22.6420	20.7870	19.8540	19.7550	0.8480	0.2100	0.0660	0.0470	0.1960
J095724.21+013159.5	149.35090	1.53321	19.99	1	3.06	0.5992	2	cos	22.3180	22.9680	21.5120	19.9900	19.5990	1.1650	0.7730	0.3610	0.1420	0.3850
J095724.98+022905.3	149.35408	2.48483	18.66	1	5.44	0.4814	3	cos	26.7010	21.3450	19.5470	18.6610	18.2400	0.7670	0.1060	0.0340	0.0280	0.0630
J095728.41+014307.4	149.36841	1.71873	19.39	3	3.11	0.0336	1	cos	24.3030	22.4020	20.5450	19.3900	18.9600	2.4410	0.2450	0.0740	0.0430	0.1180
J095728.89+021721.2	149.37040	2.28924	20.24	3	4.21	0.0008	3	cos	25.0320	22.8120	21.4660	20.2770	19.7580	1.1850	0.1700	0.0960	0.0550	0.1390
J095731.70+020327.6	149.38210	2.05768	20.39	2	2.74	0.9269	1	cos	23.0820	22.8770	22.2150	20.3910	19.6020	1.0690	0.3210	0.2880	0.0930	0.2070
J095733.18+021546.5	149.38826	2.26293	20.26	1	4.90	0.6974	3	cos	26.0990	23.2870	21.6230	20.4430	19.6990	0.9610	0.4190	0.1720	0.0980	0.2120
J095733.33+013144.5	149.38888	1.52905	20.33	1	2.52	0.6524	2	cos	23.9740	23.1710	21.3590	20.4520	19.5900	1.3940	0.2940	0.1030	0.0690	0.1170
J095734.28+025024.9	149.39286	2.84025	19.90	1	6.10	0.5540	3	cos	23.4570	22.4010	20.8830	19.9010	19.0370	1.0000	0.1950	0.0840	0.0620	0.0940
J095737.86+014333.3	149.40775	1.72593	20.44	1	3.31	0.4784	1	cos	25.9890	22.8020	21.5670	20.2210	19.4930	1.4960	0.3870	0.2040	0.1020	0.2090
J095741.91+020033.7	149.42466	2.00938	19.85	1	9.80	0.6901	4	cos	22.5380	22.3760	20.9850	19.6760	19.2900	0.6310	0.2390	0.1160	0.0600	0.1570
J095742.07+025028.4	149.42533	2.84123	19.88	1	6.65	0.5144	3	cos	22.4440	22.1470	20.7750	19.8810	19.5570	0.3270	0.1150	0.0570	0.0460	0.1090
J095742.56+023452.1	149.42734	2.58114	19.42	1	11.34	0.7019	5	cos	22.5590	22.1410	20.7490	19.4190	18.7640	0.6400	0.1740	0.0820	0.0430	0.0810
J095742.58+024432.1	149.42745	2.74228	20.11	3	5.51	0.0008	3	cos	22.6610	25.3400	21.9470	20.1110	19.6740	0.9930	2.2170	0.4110	0.1420	0.3160
J095744.56+023835.8	149.43567	2.64330	20.07	1	6.84	0.7358	3	cos	22.8760	23.2550	21.5570	20.3540	19.5620	0.6980	0.3720	0.1420	0.0830	0.1410
J095744.60+012447.1	149.43585	1.41309	20.11	3	3.97	0.0337	1	cos	25.3800	22.8650	21.7010	20.1050	19.7220	3.5850	0.6350	0.3840	0.1410	0.3750
J095745.96+014240.1	149.44153	1.71115	20.13	3	3.05	0.0002	1	cos	24.3480	22.5120	20.7400	19.5390	18.7560	3.0220	0.3360	0.1120	0.0590	0.1220
J095746.79+030025.7	149.44499	3.00716	20.08	1	3.70	0.7130	3	cos	23.1230	23.2530	20.6030	19.6350	18.8280	2.1560	0.8570	0.1320	0.0920	0.1670
J095748.08+025642.0	149.45035	2.94503	19.85	3	8.03	0.0001	3	cos	23.1270	22.3340	21.0780	19.4360	18.4770	0.9510	0.1660	0.0920	0.0350	0.0540

Table A1. The first 40 objects from the AAOmega Pilot Catalogue in RA order. The table for the full sample is available online only. [1]Using the SDSS nomenclature. [2]r-band SDSS Fibre Magnitude. [3]Model galaxy template to fit observed spectra. A value of 1 signifies the "early-type" template provided the best-fit, a value of 2 is for a $k+a$ Balmer absorption spectrum template and 3 indicates the M-star template. [4]Cross-correlation co-efficient between the model and observed galaxy spectra.